



Implementation of Substructure Flexibility and Member-Level Load Capabilities for Floating Offshore Wind Turbines in OpenFAST

Jason Jonkman,¹ Emmanuel Branlard,¹ Matthew Hall,¹
Greg Hayman,² Andy Platt,¹ and Amy Robertson¹

*1 National Renewable Energy Laboratory
2 Hayman Consulting, LLC*

**NREL is a national laboratory of the U.S. Department of Energy
Office of Energy Efficiency & Renewable Energy
Operated by the Alliance for Sustainable Energy, LLC**

This report is available at no cost from the National Renewable Energy Laboratory (NREL) at www.nrel.gov/publications.

Contract No. DE-AC36-08GO28308

Technical Report
NREL/TP-5000-76822
August 2020



Implementation of Substructure Flexibility and Member-Level Load Capabilities for Floating Offshore Wind Turbines in OpenFAST

Jason Jonkman,¹ Emmanuel Branlard,¹ Matthew Hall,¹
Greg Hayman,² Andy Platt,¹ and Amy Robertson¹

1 National Renewable Energy Laboratory

2 Hayman Consulting, LLC

Suggested Citation

Jonkman, Jason, Emmanuel Branlard, Matthew Hall, Greg Hayman, Andy Platt, Amy Robertson. 2020. *Implementation of Substructure Flexibility and Member-Level Load Capabilities for Floating Offshore Wind Turbines in OpenFAST*. Golden, CO: National Renewable Energy Laboratory. NREL/TP-5000-76822.

<https://www.nrel.gov/docs/fy20osti/76822.pdf>

**NREL is a national laboratory of the U.S. Department of Energy
Office of Energy Efficiency & Renewable Energy
Operated by the Alliance for Sustainable Energy, LLC**

This report is available at no cost from the National Renewable Energy Laboratory (NREL) at www.nrel.gov/publications.

Contract No. DE-AC36-08GO28308

Technical Report
NREL/TP-5000-76822
August 2020

National Renewable Energy Laboratory
15013 Denver West Parkway
Golden, CO 80401
303-275-3000 • www.nrel.gov

NOTICE

This work was authored in part by the National Renewable Energy Laboratory, operated by Alliance for Sustainable Energy, LLC, for the U.S. Department of Energy (DOE) under Contract No. DE-AC36-08GO28308. Funding provided by the U.S. Department of Energy Office of Energy Efficiency and Renewable Energy Wind Energy Technologies Office. The views expressed herein do not necessarily represent the views of the DOE or the U.S. Government.

This report is available at no cost from the National Renewable Energy Laboratory (NREL) at www.nrel.gov/publications.

U.S. Department of Energy (DOE) reports produced after 1991 and a growing number of pre-1991 documents are available free via www.osti.gov.

Cover Photos by Dennis Schroeder: (clockwise, left to right) NREL 51934, NREL 45897, NREL 42160, NREL 45891, NREL 48097, NREL 46526.

NREL prints on paper that contains recycled content.

Acknowledgments

This work was authored by the National Renewable Energy Laboratory, operated by the Alliance for Sustainable Energy, LLC, for the U.S. Department of Energy (DOE) under Contract No. DE-AC36-08GO28308. Funding was provided by the U.S. Department of Energy Office of Energy Efficiency and Renewable Energy under a 2018 Technology Commercialization Fund project titled “Demonstration of NREL Modeling Capability to Design the Next Generation of Floating Offshore Wind Turbines.” The views expressed in the article do not necessarily represent the views of the DOE or the U.S. Government. The U.S. Government retains and the publisher, by accepting the article for publication, acknowledges that the U.S. Government retains a nonexclusive, paid-up, irrevocable, worldwide license to publish or reproduce the published form of this work, or allow others to do so, for U.S. Government purposes.

The authors thank Henrik Stiesdal of Stiesdal A/S and Jeffrey Kenhe and Jim Lanard of Magellan Wind LLC for their support of the Technology Commercialization Fund project.

List of Acronyms

C-B	Craig-Bampton
DOE	U.S. Department of Energy
DOF	degree of freedom
HAWC2	Horizontal Axis Wind turbine simulation Code
NREL	National Renewable Energy Laboratory
OP	operating point

Executive Summary

OpenFAST is an open-source, physics-based engineering tool applicable to the load analysis of land-based and offshore wind turbines, including floating offshore wind turbines. The substructure for a floating wind turbine has historically been modeled in OpenFAST as a rigid body with hydrodynamic loads lumped at a point, which enabled the tool to predict the global response of the floating substructure but not the structural loads within its individual members. This limitation is an impediment to designing floating substructures—especially newer designs that are more streamlined, flexible, and cost-effective. This report presents the development of new functionality in OpenFAST to model floating substructure flexibility and member-level loads, as well as the concepts and mathematical background needed to understand and apply it correctly.

Table of Contents

1	Introduction	1
2	Structural Dynamics	3
2.1	Implementation Choices and Limitations.....	3
2.2	Pretensioned Cable Element.....	4
2.3	Rigid-Link Element.....	5
2.4	Rotational Joints.....	5
2.4.1	Ball Joints.....	6
2.4.2	Universal Joints.....	6
2.4.3	Pin Joints.....	6
3	Hydrodynamics	8
3.1	Member-Level Hydrostatics in the Strip-Theory Solution.....	8
3.1.1	Buoyancy on Fully Submerged Element Sides.....	9
3.1.2	Buoyancy on Partially Submerged Element Sides.....	11
3.1.3	Buoyancy on Submerged Member Ends.....	13
3.2	Multiple Potential-Flow Bodies.....	14
3.2.1	Wave Excitation.....	14
3.2.2	Wave Radiation.....	16
3.2.3	Hydrostatics.....	18
4	Coupling	19
4.1	Module-to-Module Coupling.....	19
4.2	Full-System Linearization.....	22
4.2.1	Operating Point Determination.....	22
4.2.2	Module Linearization.....	23
4.2.3	Module-to-Module Coupling Linearization.....	25
4.2.4	Final Matrix Assembly.....	28
5	Conclusions	30
	References	31

List of Figures

Figure 1.	OpenFAST and its modules.....	2
Figure 2.	Morison member discretization and lumping of distributed loads.....	8
Figure 3.	Loads on fully submerged element i lumped at node i then distributed to nodes i and $i + 1$	10
Figure 4.	Loads on partially submerged element i lumped at node i then distributed to nodes i and $i-1$..	13
Figure 5.	Change in OpenFAST control volumes for floating offshore wind turbines—before (top) and after (bottom) (BeamDyn not shown).....	20

List of Tables

Table 1.	States, Inputs, and Outputs Pertinent to Floating Substructures.....	21
----------	--	----

1 Introduction

To support innovative, optimized, reliable, and cost-effective floating offshore wind turbine designs, the wind industry and research communities rely on physics-based engineering software (i.e., design tools) capable of predicting the coupled dynamic loads and responses of the wind system. OpenFAST (formerly known as FAST), developed by the National Renewable Energy Laboratory (NREL) via support from the U.S. Department of Energy (DOE), is a state-of-the-art, open-source engineering tool (Jonkman and Sprague 2020). For floating offshore wind turbines, OpenFAST models the important physical phenomena and system couplings, including the environmental excitation (wind, waves, and current) and full-system dynamic response (rotor, drivetrain, nacelle, tower, substructure, moorings, and controller) under both normal (for fatigue) and extreme (for ultimate) loading conditions.

The substructure of a floating offshore wind turbine has historically been modeled in OpenFAST as a rigid body with hydrodynamic loads lumped at a point, which enabled the tool to predict the global response of the floating substructure but not the structural loads within its individual members. To enable the design and optimization of the floating substructures—especially next-generation floating wind technologies that show promise to be streamlined, flexible, and cost-effective—substructure flexibility and member-level load calculations have been implemented in OpenFAST. This implementation is part of a larger effort at NREL to develop an open-source, multifidelity systems analysis capability for floating offshore wind turbine analysis and optimization that captures the relevant physics and costs that drive designs and trade-offs.

To meet the modeling needs of most floating offshore wind turbine support structures—ranging from spar buoys, semisubmersibles, tension-leg platforms, and hybrid combinations of these—functional requirements for the new capability were established by reviewing existing floating offshore wind turbine prototypes and proposed concepts and comparing their structural configurations and resulting physics-based modeling needs to the modeling capabilities already available in OpenFAST, as well as new capabilities that can be implemented within the time frame and funding available for the current effort. We assessed the floating support structure—including the tower, substructure, and mooring systems—of the various floating offshore wind turbine technologies rather than innovations in the wind turbine itself, which are outside the scope of the current effort. We selected functional requirements that meet the modeling needs of most floating offshore wind turbine support structures, and we identified a few functional requirements that are important for only some floating offshore wind turbines that will require future development. We considered only modeling approaches that will maintain computational efficiency so that OpenFAST will still be capable of running the thousands of load-case simulations necessary for floating offshore wind turbine design and optimization. Jonkman et al. (2019) presents a detailed summary of the floating offshore wind turbine support structure modeling capability in OpenFAST that existed before the upgrade, the new functional requirements (including which floating offshore wind turbines these functional requirements pertain to), a qualitative description of the modeling approaches used to address the functional requirements, and functionality not considered.

This report presents the mathematical details pertinent to the modeling approaches, including structural dynamics, hydrodynamics, and their coupling. Verification of the source-code

implementation is ongoing, and results will be presented in future work to highlight the functionality and demonstrate the verification.

Note that in addition to OpenFAST, other physics-based engineering software tools have also been developed in the wind community to model the coupled dynamic responses of floating offshore wind turbines, and most of these also treat the floating substructure rigidly. Recent work by Borg et al. (2016) extended the Horizontal Axis Wind turbine simulation Code 2nd generation (HAWC2) to consider the substructure flexibility of large-volume floaters through a generalized-modes approach. The approach presented here differs from Borg et al. (2016) because large-volume bodies in floating substructures of floating offshore wind turbines are expected to be quite rigid, whereas the hydrodynamic interactions between multiple large-volume bodies and the flexibility of slender members are expected to be more significant. The approach presented here can be seen as a broader and open-source implementation of the approach taken by Luan, Gao, and Moan (2017) in Simo/Riflex/AeroDyn.

The upgrades to OpenFAST involved further development of the SubDyn structural dynamics module for substructures, the HydroDyn hydrodynamics module, and their coupling to the ElastoDyn wind turbine structural dynamics module within the OpenFAST glue (driver) code. Although SubDyn was originally developed for fixed-bottom substructures, the module is upgraded here for application to floating offshore wind turbines (HydroDyn already applies to both fixed and floating offshore wind turbines). See Figure 1 for an overview of OpenFAST and its modules.

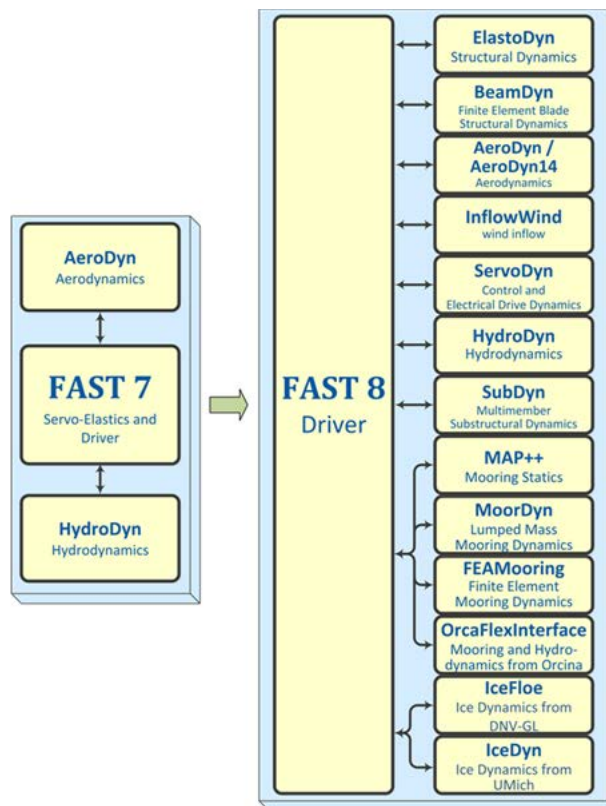


Figure 1. OpenFAST and its modules

2 Structural Dynamics

SubDyn—which models the structural dynamics of substructures using a linear beam finite-element approach together with a Craig-Bampton (C-B) reduction and Static Improvement Method. SubDyn was previously available in OpenFAST for fixed-bottom substructures, but it is now extended to model the structural flexibility and member-level loads of floating substructures. In addition to the beam elements and cantilevered interconnections previously available, new element types and interconnections important to floating substructures have been added, including pretensioned cable and rigid-link elements and pin, universal, and ball joint interconnections, referred to as rotational joints. SubDyn does not include any geometric or material nonlinearities; instead, SubDyn is inherently linear.

2.1 Implementation Choices and Limitations

Rigid links and rotational joints define linear multipoint constraints between the degrees of freedom (DOFs). The direct elimination technique is used to account for these constraints, instead of the more common and general approach of Lagrange multipliers or similar methods that result in differential algebraic equations that are difficult to time-integrate. The former technique is intuitive for simple problems and has the advantage of reducing the number of DOFs and maintaining ordinary differential equations (without algebraic constraints) that are simple to time-integrate. Yet, the direct elimination technique requires significant bookkeeping for general problems. In the current study, only a limited set of constraints is intended to be supported, and additional limitations are introduced to ease the implementation. That is, it is assumed that rigid links and pretension cables are only connected to beams at their extremities, and that the connections to the beams are cantilever joints. With these assumptions, the constraints associated with rigid links and rotational joints involve nonoverlapping sets of DOFs. Consequently, the sets of DOFs can be dealt with independently for each constraint type. The direct elimination technique (Cook 1974) consists in forming a matrix, T , and a reduced set of DOFs, \tilde{x} , such that the original DOFs, x , are expressed as:

$$x = T \tilde{x} \quad (1)$$

Each constraint, c , involves an independent subset of this equation of the form $x_c = T_c \tilde{x}_c$. The matrix T is formed by assembling the different matrices T_c (which from our assumption do not overlap), and, by introducing identity relationships for the DOFs that are not involved in any constraints, referred to as “uncommitted.” Each element used in SubDyn consists of two nodes, each node having six DOF corresponding to three translations and three rotations. A cantilever joint connecting several elements is a simple constraint, which maps all the nodal DOFs to only six DOFs for the joint. In the current implementation, the vector x is a “partially”-assembled vector of nodal DOFs, where cantilever constraints have been implicitly applied to reduce storage. After the partial assembly, the linear mass and stiffness matrices, M and K , and the force vector, F , are reduced as follows to account for the other constraints:

$$\tilde{M} = T^T M T, \quad \tilde{K} = T^T K T, \quad \tilde{F} = T^T F \quad (2)$$

where the superscript T denotes the transpose operator. Expressions for the matrices T_c will be given in the sections below for the rigid link and the rotational joints.

2.2 Pretensioned Cable Element

The finite-element representation of a pretensioned cable was obtained by defining the element with two nodes at each end of the cable extremities and by considering the balance of stresses in the element. The cable axis is assumed to be along the element axis, z . The representation consists of a specific element stiffness matrix, element mass matrix, and pretension force. The gravitational force is accounted for in a similar fashion as the beam representation and is not presented here. The user inputs for the cable element are: the undisplaced joint locations (while pretensioned), noted \mathbf{x}_1 and \mathbf{x}_2 , the pretension force, T_0 (greater than or equal to zero), and the elongation stiffness, EA . The initial element length, L , the pretension stress, ϵ_0 , and the length at zero stress, L_0 , are then respectively defined as:

$$L = \|\mathbf{x}_2 - \mathbf{x}_1\|_2, \quad \epsilon_0 = \frac{T_0}{EA}, \quad L_0 = \frac{L}{1+\epsilon_0} \quad (3)$$

With these notations, the element mass matrix, stiffness matrix, and pretension force are:

$$M_e = \rho L_0 \begin{bmatrix} 13/35 & 0 & 0 & 9/70 & 0 & 0 \\ 0 & 13/35 & 0 & 0 & 9/70 & 0 \\ 0 & 0 & 1/3 & 0 & 0 & 1/6 \\ 9/70 & 0 & 0 & 13/35 & 0 & 0 \\ 0 & 9/70 & 0 & 0 & 13/35 & 0 \\ 0 & 0 & 1/6 & 0 & 0 & 1/3 \end{bmatrix} \quad (4a)$$

$$K_e = \frac{EA}{L_0} \begin{bmatrix} \frac{\epsilon_0}{1+\epsilon_0} & 0 & 0 & -\frac{\epsilon_0}{1+\epsilon_0} & 0 & 0 \\ 0 & \frac{\epsilon_0}{1+\epsilon_0} & 0 & 0 & -\frac{\epsilon_0}{1+\epsilon_0} & 0 \\ 0 & 0 & 1 & 0 & 0 & -1 \\ -\frac{\epsilon_0}{1+\epsilon_0} & 0 & 0 & \frac{\epsilon_0}{1+\epsilon_0} & 0 & 0 \\ 0 & -\frac{\epsilon_0}{1+\epsilon_0} & 0 & 0 & \frac{\epsilon_0}{1+\epsilon_0} & 0 \\ 0 & 0 & -1 & 0 & 0 & 1 \end{bmatrix} \quad (4b)$$

$$f_e = EA\epsilon_0 \begin{Bmatrix} 0 \\ 0 \\ 1 \\ 0 \\ 0 \\ -1 \end{Bmatrix} \quad (4c)$$

where ρ is the mass per unit (unstretched) length of the cable element.

The matrices presented earlier are related to the three translational DOFs at each element extremity. The rotational DOFs are omitted here, but in the implementation, zeros are introduced at their corresponding locations in the matrices and vectors. The element variables are transformed to the global frame for the assembly in the global system, as already implemented in SubDyn.

2.3 Rigid-Link Element

Several joints may be coupled together with rigid links. A rigid assembly of n joints is here considered. Each joint, j , consists of six DOFs (from the assumption that rigid links connect to beams via cantilever joints) gathered into a vector x_j . The $6n$ DOFs of the rigid assembly can be condensed into six leader DOFs. The indexing of the joints in this paragraph is such that the first joint is selected as the leader joint. The expression of the constraint is thus:

$$x_c = T_c \tilde{x}_c \quad \text{with } x_c = \begin{Bmatrix} x_1 \\ x_2 \\ \vdots \\ x_n \end{Bmatrix} \quad \text{and } \tilde{x}_c = x_1 \quad (5)$$

For each joint $j \in \{2, \dots, n\}$, a matrix A_{1j} is formed based on the global coordinates of nodes 1 and j , noted (x_1, y_1, z_1) and (x_j, y_j, z_j) , respectively. The relation between the joint DOFs and the reduced leader DOF is then formed by stacking the A_{1j} matrices as follows:

$$T_c = \begin{bmatrix} I_6 \\ A_{12} \\ \vdots \\ A_{1n} \end{bmatrix}, \quad \text{with } A_{1j} = \begin{bmatrix} 1 & 0 & 0 & 0 & -(z_j - z_1) & -(y_j - y_1) \\ 0 & 1 & 0 & -(z_j - z_1) & 0 & -(x_j - x_1) \\ 0 & 0 & 1 & -(y_j - y_1) & -(x_j - x_1) & 0 \\ 0 & 0 & 0 & 1 & 0 & 0 \\ 0 & 0 & 0 & 0 & 1 & 0 \\ 0 & 0 & 0 & 0 & 0 & 1 \end{bmatrix} \quad (6)$$

where I_6 is the 6×6 identity matrix.

A matrix T_c is formed for each set of rigid assemblies of the system and used to build the transformation matrix T presented in Section 2.1. Rigid links may also be attributed a mass, in which case the mass matrix of a beam element is used.

2.4 Rotational Joints

A rotational joint, linking n elements of indices $[e_1, \dots, e_n]$, is considered. The $3n$ translational nodal DOFs of each element connected at the joint are lumped into three joint DOFs in the partially assembled vector x . The $3n$ rotational nodal DOFs are kept in the assembled vector, and this subset is here gathered into the vector θ_c . The matrix T_c is used to reduce the number of DOFs to an independent set of DOF and thus account for the constraint introduced by the joint.

The independent DOFs are written $\tilde{\theta}_c$ and their numbers are: $3 + 3(n - 1) = 3n$ for a ball joint, $3 + 2(n - 1) = 1 + 2n$ for a universal joint, and $3 + (n - 1) = 2 + n$ for a pin joint. The three rotational nodal DOFs of element e_j are gathered in the vector θ_{e_j} . The constraint reduction is then written as:

$$\theta_c = \begin{Bmatrix} \theta_{e_1} \\ \vdots \\ \theta_{e_n} \end{Bmatrix} = T_c \tilde{\theta}_c \quad (7)$$

The following subsections present the values of T_c and $\tilde{\theta}_c$ for each joint type.

2.4.1 Ball Joints

For a ball joint, each connected element can rotate independently in all three directions. The constraints relation is then simply determined with:

$$\tilde{\theta}_c = \theta_c = \begin{Bmatrix} \theta_{e_1} \\ \vdots \\ \theta_{e_n} \end{Bmatrix}, \quad T_c = \begin{bmatrix} I_3 & & 0 \\ & \ddots & \\ 0 & & I_3 \end{bmatrix} \quad (3n \times 3n) \quad (8)$$

where I_3 is the 3×3 identity matrix.

2.4.2 Universal Joints

Universal joints transfer the rotational moment around two misaligned axes. A universal joint, linking n elements of indices $[e_1, \dots, e_n]$, is considered. Unit vectors along the axis of each element are expressed in the global coordinate system and written \hat{z} . Similar notations are used for the unit \hat{x} and \hat{y} axes, orthogonal to the \hat{z} axis of each element, about which no moment is transferred. The DOF corresponding to the shared rotation between the axes is written $\tilde{\theta}_1$. Each element contributes two independent DOFs that are free to rotate, noted $\tilde{\theta}_x$ and $\tilde{\theta}_y$. The constraint relationship between the original DOFs and the reduced DOFs is obtained by projecting the rotational DOFs of each element against the different axes. The relations are inverted using the pseudo-inverse, defined as $A^{-1*} = A^T(AA^T)^{-1}$. The constraints are then expressed with the following variables and transformation matrix:

$$\tilde{\theta}_c = \begin{Bmatrix} \tilde{\theta}_1 \\ \tilde{\theta}_{x,e_1} \\ \tilde{\theta}_{y,e_1} \\ \vdots \\ \tilde{\theta}_{x,e_n} \\ \tilde{\theta}_{y,e_n} \end{Bmatrix}, \quad T_c = \begin{bmatrix} \hat{z}_{e_1}^T/n & \cdots & \hat{z}_{e_n}^T/n \\ \hat{x}_{e_1}^T & & 0 \\ \hat{y}_{e_1}^T & & 0 \\ 0 & \ddots & 0 \\ 0 & & \hat{x}_{e_n}^T \\ 0 & \cdots & \hat{y}_{e_n}^T \end{bmatrix}^{-1*} \quad (3n \times (1 + 2n)) \quad (9)$$

2.4.3 Pin Joints

A pin joint is characterized by a direction around which no moment is transferred. The unit vector indicating this direction is provided by the user and noted \hat{p} . Two orthogonal unit vectors \hat{p}_1 and \hat{p}_2 are then defined, forming an orthonormal basis with \hat{p} , oriented arbitrarily. The two DOFs that correspond to the shared rotations between all elements are written $\tilde{\theta}_1$ and $\tilde{\theta}_2$. Each element also has a free rotational DOF, noted $\tilde{\theta}_{e_j}$. The constraint relationship between the original DOF and the reduced DOF is obtained by projecting the rotational DOFs against the axes \hat{p}_1 , \hat{p}_2 and \hat{p} . The relations are inverted using the pseudo-inverse. The result is given as follows:

$$\tilde{\theta}_c = \begin{Bmatrix} \tilde{\theta}_1 \\ \tilde{\theta}_2 \\ \tilde{\theta}_{e_1} \\ \vdots \\ \tilde{\theta}_{e_n} \end{Bmatrix}, \quad T_c = \begin{bmatrix} \hat{p}_1^T/n & \cdots & \hat{p}_1^T/n \\ \hat{p}_2^T/n & \cdots & \hat{p}_2^T/n \\ \hat{p}^t & & 0 \\ & \ddots & \\ 0 & & \hat{p}^t \end{bmatrix}^{-1*} \quad (3n \times (2+n)) \quad (10)$$

3 Hydrodynamics

HydroDyn—which models the first- plus second-order hydrodynamics of substructures using a hybrid combination of strip theory for slender members and potential-flow theory for large-volume members—has been extended to include member-level hydrostatics in the strip-theory solution (dependent on substructure displacement) and multiple potential-flow bodies (including optional interaction between these bodies).

3.1 Member-Level Hydrostatics in the Strip-Theory Solution

The strip-theory formulation for slender members has been modified to support nonlinear hydrostatic loads, calculating buoyancy, ballast, and marine-growth loads based on the member’s instantaneous position, orientation, and deflection. The buoyancy calculations are based on the integrated pressure on the member’s submerged surface area and are exact for both cylindrical and tapered members. In addition to hydrostatic loads, other strip-theory member loads (e.g., fluid-inertia, added mass, viscous drag, water ballast, and marine growth) have also been modified in HydroDyn to account for the new discretization and to improve their accuracy. For brevity’s sake, this is not discussed in this report.

To support changes in the buoyancy load distribution as a member moves and deflects, the discretization of member loads has been changed. Each member is discretized uniformly over its length, into N elements of length dl . Members are no longer split at boundaries (i.e., at the waterplane, the water-ballast level, or the seabed). These transitions are instead handled within the load calculations of the boundary-crossing element, which can change as a member moves. Loads are now calculated in lumped form for each element. The loads on element i are formulated with respect to node i and then spread by factor α to node $i + 1$, as illustrated in Figure 2.

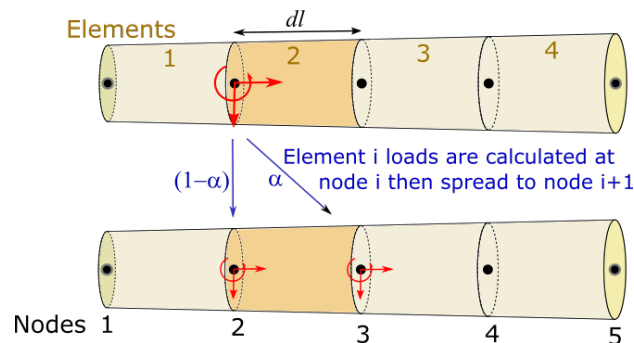


Figure 2. Morison member discretization and lumping of distributed loads

Each member has $N+1$ nodes. The member’s starting and ending radii are denoted r_1 and r_{N+1} , respectively, and the vertical elevations (relative to the still level waterplane) of these nodes are Z_1 and Z_{N+1} , respectively. The variable l indicates the coordinate along the length of the member in a relative sense.

Because users may specify depth-dependent marine growth thicknesses, the nodes along each strip-theory member are individually assigned a marine growth thickness, $t_{MG,i}$, and marine

growth density based on their depth at initialization. The member radius inclusive of the marine growth at node i is:

$$r_{MG,i} = r_i + t_{MG,i} \quad (11)$$

The presence of marine growth means that the outer surface of each element along a member may be tapered uniquely, regardless of whether the member itself is tapered. The taper ratio ($m = dr/dl$) of each element is calculated as:

$$m_i = \frac{(r_{i+1} + t_{MG,i+1}) - (r_i + t_{MG,i})}{dl} \quad (12)$$

Loads are distributed based on the relative position of an element's volumetric centroid between its two nodes. For a fully submerged cylindrical element that may be tapered and may have marine growth, the relative position of the centroid between node i and node $i + 1$ is:

$$\alpha_i = \frac{(r_i + t_{MG,i})^2 + 2(r_i + t_{MG,i})(r_{i+1} + t_{MG,i+1}) + 3(r_{i+1} + t_{MG,i+1})^2}{4[(r_i + t_{MG,i})^2 + (r_i + t_{MG,i})(r_{i+1} + t_{MG,i+1}) + (r_{i+1} + t_{MG,i+1})^2]} \quad (13)$$

where $\alpha_i = 0$ corresponds to the centroid being at node i and $\alpha_i = 1$ corresponds to the centroid being at node $i + 1$ (but typically α_i falls within these limits). The quantities m_i and α_i are calculated for each element in the member at initialization in the reference (undisplaced) configuration.

To simplify the calculations, hydrostatic loads are derived based on a two-dimensional representation and then converted back into three dimensions afterward. The member's inclination angle from vertical is denoted ϕ and the heading of the incline is β (although both of these angles may vary across elements when the member is deflected, indicated by subscript i). These are both calculated at every time step in the formulation that follows.

Buoyancy loads are calculated differently for fully submerged and partially submerged elements. To avoid an abrupt (step) change in forces and moments when a node crosses the waterline, smoothing techniques are used and loads on a partially submerged element are lumped at the two closest nodes below the waterline.

3.1.1 Buoyancy on Fully Submerged Element Sides

The buoyancy loads on fully submerged elements are calculated based on the solution of a pressure integration around the side wall of the element. The net axial (l) force, transverse (r) force, and moment (about node i) on element i are:

$$F_l = -2 \pi m_i \rho g dl \left(Z_i r_{MG,i} + \frac{1}{2} (Z_i m_i + r_{MG,i} \cos \phi_i) dl + \frac{1}{3} m_i \cos \phi_i dl^2 \right) \quad (14)$$

$$F_r = -\pi \rho g dl \left(r_{MG,i}^2 + m_i r_{MG,i} dl + \frac{1}{3} m_i^2 dl^2 \right) \sin \phi_i \quad (15)$$

$$\begin{aligned}
M_0 = & -\pi \rho g dl \left(\frac{1}{4} dl^3 m_i^4 + \frac{1}{4} dl^3 m_i^2 + dl^2 m_i^3 r_{MG,i} \right. \\
& + \frac{2}{3} dl^2 m_i r_{MG,i} + \frac{3}{2} dl m_i^2 r_{MG,i}^2 + \frac{1}{2} dl r_{MG,i}^2 \\
& \left. + m_i r_{MG,i}^3 \right) \sin \phi_i
\end{aligned} \tag{16}$$

where ρ is the water density and g is the gravitational acceleration. These loads are illustrated in Figure 3.

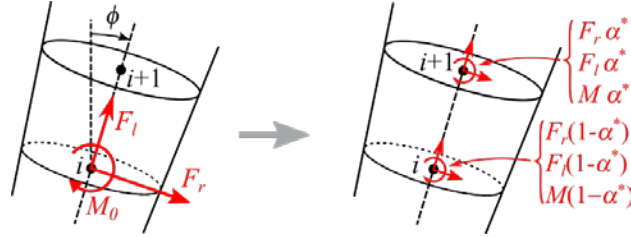


Figure 3. Loads on fully submerged element i lumped at node i then distributed to nodes i and $i + 1$

Once the force components and moment are calculated for the element, they are distributed between the adjacent nodes based on the relative location of the element's center of buoyancy (submerged centroid) and the nodes' water depths. The distribution factor is¹:

$$\alpha_i^* = \frac{\alpha_i Z_{i+1}^3}{(1-\alpha_i)Z_i^3 + \alpha_i Z_{i+1}^3} \tag{17}$$

noting that $Z_i < 0$ and $Z_{i+1} < 0$ for a fully submerged element. The distribution factor α_i^* approaches α_i as the depth of the element increases. The resulting force distributions are of the form $F_{i+1} = F\alpha_i^*$ and $F_i = F(1 - \alpha_i^*)$, where F is any force or moment mentioned above.

Before distributing the moment, it must be adjusted to compensate for the moment created when distributing the radial force component:

$$M = M_0 - F_r \alpha_i^* dl \tag{18}$$

Lastly, the heading and inclination angle must be applied to convert the loads into the global coordinate system:

¹ The cube exponent is used for smoothing and may be adjusted after further exploration.

$$C_2 = a_h b_h r_h \cos \phi_i - r_{MG,i}^3 \quad (26)$$

These equations hold whether the taper is positive or negative and also provide the desired effect when the definition of the submerged volume includes a negative-volume region (i.e., when the plate at node i is only partially submerged); however, they are not defined for a nontapered cylinder.

For a nontapered cylinder, the calculations are based on a truncated cylinder geometry:

$$V = \pi r_{MG,i}^2 h \quad (27)$$

$$r_c = \frac{1}{4} \frac{r_{MG,i}^2 \tan \phi_i}{h} \quad (28)$$

$$h_c = \frac{1}{2} h + \frac{1}{8} \frac{r_{MG,i}^2 \tan^2 \phi_i}{h} \quad (29)$$

Once the displacement volume characteristics are known, the buoyancy force and moment are calculated based on the displaced volume and the horizontal offset of its centroid relative to node i :

$$x_c = r_c \cos \phi_i + h_c \sin \phi_i \quad (30)$$

Because the element is part of a larger member, only the portion of load resulting from the pressure around the side wall of the element should be used. The contribution from the bottom plate that would be exposed to the water if the element were in isolation must be subtracted (this is done in the second terms in F_l and M_0 below). The total displacement-based forces and moments from element i acting about node i are therefore:

$$F_l = \rho g (V \cos \phi_i + \pi r_{MG,i}^2 Z_i) \quad (31)$$

$$F_r = -\rho g V \sin \phi_i \quad (32)$$

$$M_0 = \rho g \left(-V x_c + \frac{\pi}{4} r_{MG,i}^4 \sin \phi_i \right) \quad (33)$$

These loads need to be distributed to nodes in a continuous way, even as elements transition in and out of the water. This is done by modifying the original centroid-based distribution according to the nodes' elevations, such that the force or moment goes to zero when a node is at or above the waterplane. The element's loads are distributed to the element's lower node and to the node below that one, as depicted in Figure 4. Noting that $Z_i < 0$ and $Z_{i+1} \geq 0$ for a partially submerged element, the modified distribution factor is calculated as²:

² The cube exponent is used for smoothing and may be adjusted after further exploration.

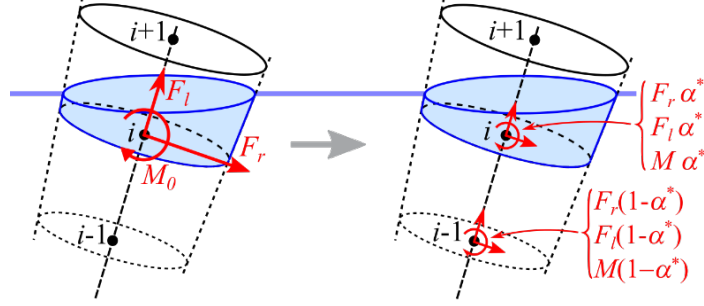


Figure 4. Loads on partially submerged element i lumped at node i then distributed to nodes i and $i-1$

$$\alpha_i^* = \frac{(1-\alpha_i)Z_i^3}{(1-\alpha_i)Z_i^3 - \alpha_i Z_{i+1}^3} \quad (34)$$

and the loads from element i are distributed according to $F_i = F \alpha_i^*$ and $F_{i-1} = F(1 - \alpha_i^*)$.

As with the fully submerged case, the moment needs to be adjusted to account for the distribution of the radial force down the member. Because the forces are shifted down an element length, the corrected moment is:

$$M = M_0 + F_r(1 - \alpha_i^*) dl \quad (35)$$

The last step is to convert back into global coordinates based on the heading of the member's incline, following the same approach as for the fully flooded elements (20).

This approach to the buoyancy loads provides exact net buoyancy quantities but is limited to members that are either fully submerged or partially submerged. Transitioning between the two states—i.e., an end element of a member crossing the water plane—is not supported. The load distribution accuracy improves with finer discretizations. The computation process is done member by member and element by element, with each element adding forces to the applicable nodes. Joint nodes attached to multiple members will then see forces from each member.

3.1.3 Buoyancy on Submerged Member Ends

The buoyancy forces and moments on submerged member ends are calculated as follows:

$$\vec{F}_{B_{end,1}} = \begin{Bmatrix} F_l \sin \phi_i \cos \beta_i \\ F_l \sin \phi_i \sin \beta_i \\ F_l \cos \phi_i \\ -M \sin \beta_i \\ M \cos \beta_i \\ 0 \end{Bmatrix}, \quad \vec{F}_{B_{end,N+1}} = \begin{Bmatrix} -F_l \sin \phi_i \cos \beta_i \\ -F_l \sin \phi_i \sin \beta_i \\ -F_l \cos \phi_i \\ M \sin \beta_i \\ -M \cos \beta_i \\ 0 \end{Bmatrix} \quad (36)$$

where the axial force and moment terms are:

$$F_l = -\rho g \pi r_{MG,i}^2 Z_i \quad (37)$$

$$M = -\rho g \frac{\pi}{4} r_{MG,i}^4 \sin \phi_i \quad (38)$$

If the member is only partially submerged, then the buoyancy load on the upper end ($N + 1$) is instead set to zero.

3.2 Multiple Potential-Flow Bodies

HydroDyn now supports multiple potential-flow bodies that can move relative to each other. Each body can have its own set of frequency-dependent hydrodynamic data files (typically generated by WAMIT (Lee and Newman 2006); the hydrodynamic data files are assumed by HydroDyn to be in WAMIT format regardless), or when considering full hydrodynamic interaction, the multiple bodies can have one common set of hydrodynamic data files (calculated via what is called the “NBody” option in WAMIT). The approach is dictated in HydroDyn by a flag called NBodyMod.

When NBodyMod is set to 1, this indicates full hydrodynamic interaction (coupling) between the N bodies. A single set of hydrodynamic data is used for the bodies, meaning coupling terms are included. The hydrodynamic data has $6N$ load components and $6N$ modes of motion (surge, sway, heave, roll, pitch, and yaw for each body).

When NBodyMod is set to 2 or 3, coupling terms between the bodies are neglected. In these cases, each body will have a distinct set of hydrodynamic data for its own six loads and six modes of motion. The case with NBodyMod set to 2 requires frequency-domain potential-flow analyses to use bodies centered at the origin rather than at their displaced and rotated locations within the substructure. The offset of the bodies relative to the tower centerline is then applied through transformations performed within HydroDyn. This can be used to model large-volume bodies whose reference point is offset from the turbine tower. The case with NBodyMod set to 3 requires the frequency-domain potential-flow analyses to use bodies already offset to their proper positions within the substructure. No further offsets are applied in HydroDyn. Neglecting hydrodynamic interaction between the bodies is often acceptable (depending on the volume of, and spacing between, the bodies) and reduces computational expense.

Regardless of the NBodyMod setting, whenever a body has a nonzero heading relative to the substructure reference coordinate system, the hydrodynamic data needs to undergo a rotational transformation. If θ is the heading angle of the body, the rotation matrix from the global reference frame to the body’s heading is

$$\mathbf{R} = \begin{bmatrix} \cos \theta & \sin \theta & 0 \\ -\sin \theta & \cos \theta & 0 \\ 0 & 0 & 1 \end{bmatrix} \quad (39)$$

The handling of Fourier-transform-based wave excitation, convolution-based wave radiation, and hydrostatics for multiple potential-flow bodies are described in the upcoming sections. Similar adjustments for state-space-based wave excitation and radiation for multiple potential-flow bodies have also been implemented but are excluded here for brevity.

3.2.1 Wave Excitation

Because wave-excitation coefficients do not involve any interaction between load components, no adjustments are required in how these coefficients are structured. For N bodies, there are $6N$ wave-excitation coefficients, six for each body.

$$\vec{\underset{6N}{X}}(\omega, \beta) = \left\{ \begin{array}{c} \vec{\underset{6}{X}}_1(\omega, \beta) \\ \vec{\underset{6}{X}}_2(\omega, \beta) \\ \vdots \\ \vec{\underset{6}{X}}_N(\omega, \beta) \end{array} \right\} = \left\{ \begin{array}{c} X_1(\omega, \beta) \\ X_2(\omega, \beta) \\ \vdots \\ X_{6N}(\omega, \beta) \end{array} \right\} \quad (40)$$

where ω is the wave frequency, β is the wave heading and each body's coefficients are:

$$\vec{X}_n(\omega, \beta) = \left\{ \begin{array}{c} X_1^{local}(\omega, \beta) \\ X_2^{local}(\omega, \beta) \\ \vdots \\ X_6^{local}(\omega, \beta) \end{array} \right\}_{\text{body } n} \quad (41)$$

The hydrodynamic data in WAMIT output files are oriented with the body, so the wave-excitation vector must be transformed to give output in the global orientation frame:

$$\vec{X}_n(\omega, \beta) = \left\{ \begin{array}{l} \mathbf{R}^\top \left\{ \begin{array}{c} X_1^{local}(\omega, \beta) \\ X_2^{local}(\omega, \beta) \\ X_3^{local}(\omega, \beta) \end{array} \right\} \\ \mathbf{R}^\top \left\{ \begin{array}{c} X_4^{local}(\omega, \beta) \\ X_5^{local}(\omega, \beta) \\ X_6^{local}(\omega, \beta) \end{array} \right\} \end{array} \right\} = \left\{ \begin{array}{c} X_1^{local}(\omega, \beta) \cos \theta - X_2^{local}(\omega, \beta) \sin \theta \\ X_1^{local}(\omega, \beta) \sin \theta + X_2^{local}(\omega, \beta) \cos \theta \\ X_3^{local}[\omega, \beta] \\ X_4^{local}(\omega, \beta) \cos \theta - X_5^{local}(\omega, \beta) \sin \theta \\ X_4^{local}(\omega, \beta) \sin \theta + X_5^{local}(\omega, \beta) \cos \theta \\ X_6^{local}(\omega, \beta) \end{array} \right\} \quad (42)$$

When NBodyMod is set to 2, additional adjustments are needed to account for the offsets and heading of each body because the wave-excitation data in this case is based on each body being centered and unrotated at the origin. The offset is achieved with a phase shift in the wave-excitation frequency components to adjust the incident wave point from the global origin to a different (undisplaced) location (X, Y) . For first-order excitation, this phase shift is:

$$F_{XY}^{(1)}(\omega, X, Y) = e^{-j k(\omega) (X \cos \beta(\omega) + Y \sin \beta(\omega))} \quad (43)$$

where $k(\omega)$ is the wave number. The heading adjustment is made by using $\beta^* = \beta - \theta$ when identifying wave-excitation coefficients from the hydrodynamic tables (for the other NBodyMod cases, $\beta^* = \beta$ and $X = Y = 0$).

The overall adjustment for any six-component set of first-order wave-excitation coefficients is:

$$\vec{X}_n(\omega, \beta) = \begin{cases} X_1^{local}(\omega, \beta^*) \cos \theta - X_2^{local}(\omega, \beta^*) \sin \theta \\ X_1^{local}(\omega, \beta^*) \sin \theta + X_2^{local}(\omega, \beta^*) \cos \theta \\ X_3^{local}(\omega, \beta^*) \\ X_4^{local}(\omega, \beta^*) \cos \theta - X_5^{local}(\omega, \beta^*) \sin \theta \\ X_4^{local}(\omega, \beta^*) \sin \theta + X_5^{local}(\omega, \beta^*) \cos \theta \\ X_6^{local}(\omega, \beta^*) \end{cases} F_{XY}^{(1)}(\omega, X, Y) \quad (44)$$

Once the first-order wave-excitation coefficients have been adjusted, the time-dependent wave-excitation forces are calculated just as they were in prior versions of HydroDyn. That is, the first-order wave-excitation coefficients are multiplied by the discrete Fourier transform of the time-dependent wave elevation at the global origin and an inverse discrete Fourier transform is used to calculate the wave-excitation load time series for each load component (size $6N$ for multiple bodies).

The application of multiple bodies for second-order wave excitation follows an analogous approach to that for first-order excitation.

3.2.2 Wave Radiation

The handling of the wave-radiation forces depends on the setting of NBodyMod.

When NBodyMod is 1 (multiple bodies with full hydrodynamic coupling), two nonsparse global matrices are needed for added mass (**A**) and damping (**B**). Each is of size $6N \times 6N$ to represent the interactions of every mode of motion of every body:

$$\underset{6N \times 6N}{\mathbf{A}}(\omega) = \begin{bmatrix} \underbrace{\mathbf{A}_{11}}_{6 \times 6}(\omega) & \underbrace{\mathbf{A}_{12}}_{6 \times 6}(\omega) & \cdots & \underbrace{\mathbf{A}_{1N}}_{6 \times 6}(\omega) \\ \underbrace{\mathbf{A}_{21}}_{6 \times 6}(\omega) & \underbrace{\mathbf{A}_{22}}_{6 \times 6}(\omega) & \cdots & \underbrace{\mathbf{A}_{2N}}_{6 \times 6}(\omega) \\ \vdots & \vdots & \ddots & \vdots \\ \underbrace{\mathbf{A}_{N1}}_{6 \times 6}(\omega) & \underbrace{\mathbf{A}_{N2}}_{6 \times 6}(\omega) & \cdots & \underbrace{\mathbf{A}_{NN}}_{6 \times 6}(\omega) \end{bmatrix} \quad (45)$$

where ω is the body oscillation frequency and each diagonal submatrix is the 6×6 matrix of each body (the effect of the body's modes of motion on itself) and each off-diagonal submatrix represent couplings between bodies (the effect of one body on another).

When NBodyMod is 2 or 3, (multiple bodies treated as hydrodynamically independent), there are no off-diagonal submatrices in the global added mass or damping matrices and these matrices are instead just composed of individual matrices for each body, for example:

$$\underset{6N \times 6N}{\mathbf{A}}(\omega) = \begin{bmatrix} \underbrace{\mathbf{A}_1}_{6 \times 6}(\omega) & \mathbf{0}_{6 \times 6} & \cdots & \mathbf{0}_{6 \times 6} \\ \mathbf{0}_{6 \times 6} & \underbrace{\mathbf{A}_2}_{6 \times 6}(\omega) & \cdots & \mathbf{0}_{6 \times 6} \\ \vdots & \vdots & \ddots & \vdots \\ \mathbf{0}_{6 \times 6} & \mathbf{0}_{6 \times 6} & \cdots & \underbrace{\mathbf{A}_N}_{6 \times 6}(\omega) \end{bmatrix} \quad (46)$$

In this situation, each body's radiation calculations are handled independently through N distinct 6×6 matrix calculations.

Because the wave-radiation retardation-kernel matrix is calculated from the frequency-dependent damping matrix, its structure follows that of the damping matrix. For coupled bodies, it is a single global $6N \times 6N$ matrix. For uncoupled bodies, it is N distinct 6×6 matrices.

In all NBodyMod cases, when a body's heading is nonzero, a correction must be made to transform the matrices from local to global coordinates. This can be done by transforming each 6×6 added mass and damping submatrix individually. In the following transformation, \mathbf{R}_i and \mathbf{R}_j are the rotation matrices for the headings of body i and body j , respectively. When NBodyMod is 2 or 3, only the diagonal submatrices are used so $i = j$.

$$\underbrace{\mathbf{A}_{ij}}_{6 \times 6}(\omega) = \begin{bmatrix} \mathbf{R}_i^\top \begin{bmatrix} a_{11}(\omega) & a_{12}(\omega) & a_{13}(\omega) \\ a_{21}(\omega) & a_{22}(\omega) & a_{23}(\omega) \\ a_{31}(\omega) & a_{32}(\omega) & a_{33}(\omega) \end{bmatrix}_{ij} \mathbf{R}_j & \mathbf{R}_i^\top \begin{bmatrix} a_{14}(\omega) & a_{15}(\omega) & a_{16}(\omega) \\ a_{24}(\omega) & a_{25}(\omega) & a_{26}(\omega) \\ a_{34}(\omega) & a_{35}(\omega) & a_{36}(\omega) \end{bmatrix}_{ij} \mathbf{R}_j \\ \mathbf{R}_i^\top \begin{bmatrix} a_{41}(\omega) & a_{42}(\omega) & a_{43}(\omega) \\ a_{51}(\omega) & a_{52}(\omega) & a_{53}(\omega) \\ a_{61}(\omega) & a_{62}(\omega) & a_{63}(\omega) \end{bmatrix}_{ij} \mathbf{R}_j & \mathbf{R}_i^\top \begin{bmatrix} a_{44}(\omega) & a_{45}(\omega) & a_{46}(\omega) \\ a_{54}(\omega) & a_{55}(\omega) & a_{56}(\omega) \\ a_{64}(\omega) & a_{65}(\omega) & a_{66}(\omega) \end{bmatrix}_{ij} \mathbf{R}_j \end{bmatrix} \quad (47)$$

Wave radiation calculations in the time domain for multiple bodies requires applying the standard linear hydrodynamics (Cummins) equation to the appropriate form of the coefficients. The generic equation for wave radiation loads is:

$$\vec{F}^{Radiation}(t) = -\mathbf{A}^\infty \ddot{\vec{q}}(t) - \int_0^t \mathbf{K}(t - \tau) \dot{\vec{q}}(\tau) d\tau \quad (48)$$

where $\mathbf{A}^\infty = \mathbf{A}(\infty)$ is the added mass matrix at infinite frequency and each element of the wave radiation retardation kernel, $\mathbf{K}(t)$, is calculated using a cosine transform:

$$\mathbf{K}_{ij}(t) = \frac{2}{\pi} \int_0^\infty \mathbf{B}_{ij}(\omega) \cos(\omega t) d\omega \quad (49)$$

If hydrodynamic interactions between bodies are included (NBodyMod set to 1), Eq. 48 is applied to the global vectors and matrices to give the full list of $6N$ radiation forces/moments:

$$\begin{bmatrix} \vec{F}_1^{Radiation}(t) \\ \vec{F}_2^{Radiation}(t) \\ \vdots \\ \vec{F}_{6N}^{Radiation}(t) \end{bmatrix} = - \begin{bmatrix} \mathbf{A}_{11}^\infty & \mathbf{A}_{12}^\infty & \cdots & \mathbf{A}_{1N}^\infty \\ \mathbf{A}_{21}^\infty & \mathbf{A}_{22}^\infty & \cdots & \mathbf{A}_{2N}^\infty \\ \vdots & \vdots & \ddots & \vdots \\ \mathbf{A}_{N1}^\infty & \mathbf{A}_{N2}^\infty & \cdots & \mathbf{A}_{NN}^\infty \end{bmatrix} \begin{bmatrix} \ddot{\vec{q}}_1(t) \\ \ddot{\vec{q}}_2(t) \\ \vdots \\ \ddot{\vec{q}}_N(t) \end{bmatrix} - \int_0^t \begin{bmatrix} \mathbf{K}_{11}(t - \tau) & \mathbf{K}_{12}(t - \tau) & \cdots & \mathbf{K}_{1N}(t - \tau) \\ \mathbf{K}_{21}(t - \tau) & \mathbf{K}_{22}(t - \tau) & \cdots & \mathbf{K}_{2N}(t - \tau) \\ \vdots & \vdots & \ddots & \vdots \\ \mathbf{K}_{N1}(t - \tau) & \mathbf{K}_{N2}(t - \tau) & \cdots & \mathbf{K}_{NN}(t - \tau) \end{bmatrix} \begin{bmatrix} \dot{\vec{q}}_1(\tau) \\ \dot{\vec{q}}_2(\tau) \\ \vdots \\ \dot{\vec{q}}_N(\tau) \end{bmatrix} d\tau \quad (50)$$

For bodies with independent hydrodynamics (NBodyMod set to 2 or 3), Eq. 48 is applied to each body separately; each body undergoes a process that is essentially the same as the previously available single-body radiation force calculation.

3.2.3 Hydrostatics

Hydrostatics data and calculations follow the form of the wave-radiation matrices as determined by N and NBodyMod. When NBodyMod is 1, the hydrostatic matrix is expanded to have $6N$ rows and columns. When NBodyMod is 2 or 3, distinct hydrostatic matrices are used for each body. Each row or column of the hydrostatic coefficient matrix/matrices corresponds to a load component or mode of motion in the respective body's local coordinate system. Accordingly, the hydrostatic submatrices, \mathbf{C}_{ij} , are transformed similarly to the added mass and damping matrices:

$$\underbrace{\mathbf{C}_{ij}}_{6 \times 6} = \begin{bmatrix} \mathbf{R}_i^\top \begin{bmatrix} c_{11} & c_{12} & c_{13} \\ c_{21} & c_{22} & c_{23} \\ c_{31} & c_{32} & c_{33} \end{bmatrix}_{ij} \mathbf{R}_j & \mathbf{R}_i^\top \begin{bmatrix} c_{14} & c_{15} & c_{16} \\ c_{24} & c_{25} & c_{26} \\ c_{34} & c_{35} & c_{36} \end{bmatrix}_{ij} \mathbf{R}_j \\ \mathbf{R}_i^\top \begin{bmatrix} c_{41} & c_{42} & c_{43} \\ c_{51} & c_{52} & c_{53} \\ c_{61} & c_{62} & c_{63} \end{bmatrix}_{ij} \mathbf{R}_j & \mathbf{R}_i^\top \begin{bmatrix} c_{44} & c_{45} & c_{46} \\ c_{54} & c_{55} & c_{56} \\ c_{64} & c_{65} & c_{66} \end{bmatrix}_{ij} \mathbf{R}_j \end{bmatrix} \quad (51)$$

Because there is never hydrostatic coupling between bodies ($\mathbf{C}_{ij} = 0$ when $i \neq j$), no further change is needed in how hydrostatic forces are calculated, regardless of the NBodyMod setting. The hydrostatic matrix is multiplied by the displacement/rotation vector/vectors in global coordinates after the hydrostatic matrix has been expressed in global coordinates.

$$\vec{F}^{Hydrostatic}(t) = \vec{F}_0^{Hydrostatic} - \mathbf{C} \vec{q}(t) \quad (52)$$

where—for each body—the hydrostatic force and moments at the platform's undisplaced position are changed to account for each body's offset position:

$$\vec{F}_0^{Hydrostatic} = \rho g \nabla_0 \begin{Bmatrix} 0 \\ 0 \\ 1 \\ (Y^{COB} - Y) \\ -(X^{COB} - X) \\ 0 \end{Bmatrix} \quad (53)$$

where ∇_0 is the undisplaced volume of the body and X^{COB} and Y^{COB} are the undisplaced body's center of buoyancy relative to the global origin.

4 Coupling

The OpenFAST glue code—which connects the modules to enable coupled aero-hydro-servo-elastic interactions—was extended to ensure the new functionality within SubDyn and HydroDyn is properly coupled together with the other OpenFAST modules. The new functionality applies to both nonlinear time-domain solutions and full-system linearization.

4.1 Module-to-Module Coupling

The modules of OpenFAST (SubDyn, HydroDyn, and so on) correspond to different physical domains of the coupled aero-hydro-servo-elastic solution, most of which are separated by spatial boundaries. Figure 5 shows how the control volumes associated with each module for floating offshore wind turbines change with the addition of floating platform flexibility and member-level loads. Though not shown, finite-element blade structural dynamics are optionally available through the BeamDyn module. Previously, SubDyn had been used only for fixed-bottom wind turbines, but this has been changed to allow SubDyn to be enabled for floating offshore wind turbines.

When SubDyn is enabled for floating offshore wind turbines, the coupling between the flexible substructure and the wind turbine, the coupling between the flexible substructure and hydrodynamic loads, and the coupling between the flexible substructure and the mooring reaction loads is modeled in the OpenFAST glue code as follows (the first two items are identical to coupling previously available for bottom-fixed offshore wind turbines, but the last item is new):

- SubDyn receives the motions (including accelerations) of the boundary nodes at the top of the substructure (transition piece), which is coincident with the tower base/platform from ElastoDyn, and ElastoDyn receives the substructure reaction loads from SubDyn at each coupling time step. It is also possible to model the entire support structure with SubDyn such that the coupling to ElastoDyn is at the yaw bearing/nacelle (eliminating the tower and rigid platform from ElastoDyn), but geometric nonlinearities are then absent from the support structural dynamics.
- HydroDyn receives the motions (including accelerations) of the flexible substructure from SubDyn, and SubDyn receives the hydrodynamic loads from HydroDyn at each coupling time step.
- The mooring module (MAP++, MoorDyn, or FEAMooring) receives the position of the fairleads from SubDyn, and SubDyn receives the reaction loads (tensions) at each fairlead from the mooring module at each coupling time step.

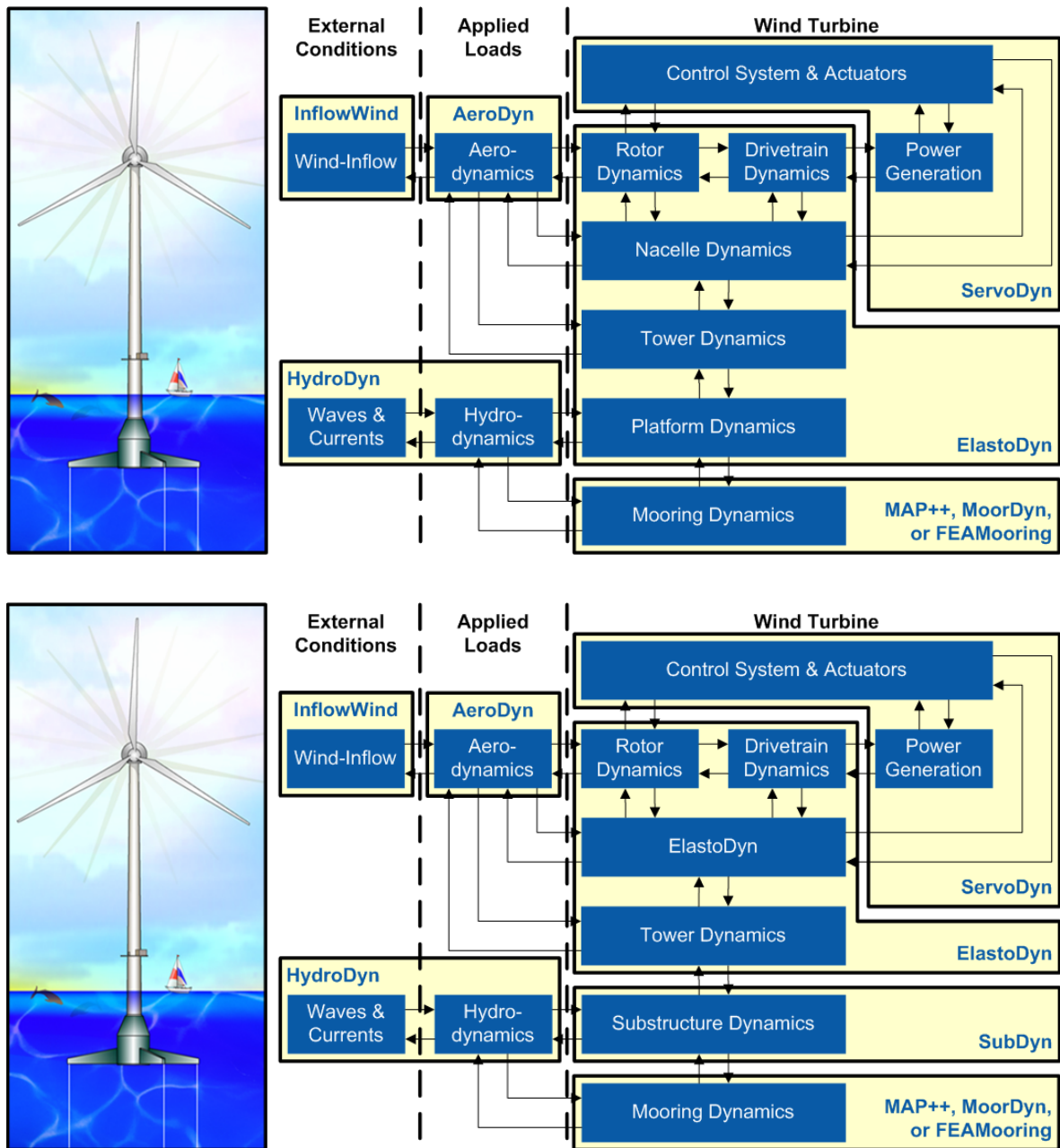


Figure 5. Change in OpenFAST control volumes for floating offshore wind turbines—before (top) and after (bottom) (BeamDyn not shown)

The inputs and outputs of ElastoDyn, HydroDyn, SubDyn, and MAP++ pertinent to floating substructure coupling are summarized in Table 1 (the internal module states also shown in Table 1 are discussed in the next subsection). Each of these inputs and outputs reside on a spatial boundary, which in the FAST modularization framework are defined in terms of a mesh. The module-to-module, input-output coupling relationships in the OpenFAST glue code are algebraic and include spatial mesh-to-mesh mappings.

Table 1. States, Inputs, and Outputs Pertinent to Floating Substructures

Module	States	Inputs	Outputs
ElastoDyn (ED)	<ul style="list-style-type: none"> • Position and orientation and translational and rotational velocities of the transition piece (continuous states) 	<ul style="list-style-type: none"> • Applied point forces and moments lumped on the transition piece 	<ul style="list-style-type: none"> • Translational displacements, orientations, translational and rotational velocities, and translational and rotation accelerations of the transition piece • User-selected structural outputs
HydroDyn (HD)	<ul style="list-style-type: none"> • State-space-based wave-excitation states (continuous states) • State-space-based wave-radiation states (continuous states) 	<ul style="list-style-type: none"> • Translational displacements, orientations, translational and rotational velocities, and translational and rotational accelerations of strip-theory analysis nodes distributed along the substructure • Translational displacements, orientations, translation and rotational velocities, and translational and rotational accelerations of potential-flow bodies • Disturbance of wave elevation at the platform reference point 	<ul style="list-style-type: none"> • Hydrodynamic-applied point forces and moments at strip-theory analysis nodes distributed along the substructure • Hydrodynamic-applied point forces and moments at each potential-flow body • User-selected hydrodynamic outputs
SubDyn (SD)	<ul style="list-style-type: none"> • Displacements and velocities of the substructure Craig-Bampton modes (continuous states) 	<ul style="list-style-type: none"> • Translational displacements, orientations, translational and rotational velocities, and translational and rotation accelerations of the transition piece • Applied point forces and moments at finite-element nodes distributed along the substructure 	<ul style="list-style-type: none"> • Reaction point forces and moments lumped at the transition piece • Translational displacements, orientations, translational and rotational velocities, and translational and rotational accelerations of finite-element nodes distributed along the substructure • User-selected structural outputs
MAP++ (MAP)	<ul style="list-style-type: none"> • Horizontal and vertical tensions at the fairlead of each mooring line (constraint states) • Positions of each connect node (constraint states for multisegmented mooring) 	<ul style="list-style-type: none"> • Translational displacements of each fairlead 	<ul style="list-style-type: none"> • Reaction point forces (tensions) lumped at each fairlead • User-selected mooring outputs

4.2 Full-System Linearization

While most physics involved in wind energy are linear, linearization of the underlying nonlinear wind-system equations is often important for understanding the system response and exploiting well-established methods and tools for analyzing linear systems. Previous OpenFAST linearization work focused on: (1) structuring the OpenFAST source code to enable linearization; (2) developing the general approach to linearizing the mesh mapping within the module-to-module, input-output coupling relationships, including rotations; (3) linearizing core (but not all features) of the land-based and floating offshore modules of OpenFAST for rigid substructures (InflowWind, AeroDyn, ServoDyn, ElastoDyn, BeamDyn, HydroDyn, MAP++) and their coupling; and (4) verifying this implementation by applying the tool to sample cases (Jonkman and Jonkman 2016; Jonkman, Jonkman, and Platt forthcoming; Jonkman et al. 2018; Johnson et al. 2019). This work extends these efforts to SubDyn, the recent extensions to HydroDyn, and their coupling.

The overall linearization approach that the FAST modularization framework was designed to support is explained in Jonkman (2013) and is consistent with the present implementation. Details on prior linearization development and verification is explained in Jonkman and Jonkman (2016); Jonkman, Jonkman, and Platt (forthcoming); Jonkman et al. (2018); and Johnson et al. (2019). Without replicating most of the information, this section uses the same approach and nomenclature of Jonkman and Jonkman (2016), Jonkman, Jonkman, and Platt (forthcoming), Jonkman et al. (2018), and Johnson et al. (2019), adding details about the linearization of the new functionality in OpenFAST to model floating substructure flexibility and member-level loads. While not the focus of the present work, due the addition of SubDyn to the list of linearizable modules within OpenFAST, the new linearization functionality of OpenFAST also applies for the first time to bottom-fixed offshore wind turbines with flexible substructures.

The linearization of OpenFAST involves: (1) finding an operating point (OP); (2) linearizing the underlying nonlinear equations of each module about the OP; (3) linearizing the module-to-module input-output coupling relationships in the OpenFAST glue code about the OP; and (4) combining all linearized matrices into the full-system linear state-space model and exporting those matrices and the OP to a file. Each step is highlighted in the following subsections.

4.2.1 Operating Point Determination

OP (or fixed-point) determination is an important first step in the linearization process because a linear representation of a nonlinear system is only valid for small deviations (perturbations) from an OP. In the current release of OpenFAST, an OP can be defined by given initial conditions (time zero) or a given time (or times) in the nonlinear time-marching process. Work is ongoing in parallel to the present effort to automate the OP determination, including trim of control inputs (but is out of the scope of this report). It is usually important for the OP to be a static-equilibrium condition (for parked/idling turbines) or steady-state condition (for operating turbines); otherwise, it may have an undesirable effect on the linear system matrices.

An OP is defined by given values for the continuous time states, $x|_{op}$, discrete-time states, $x^d|_{op}$, inputs, $u|_{op}$, and time, $t|_{op}$, for each module. Equations 1a, 1c, and 1d from Jonkman (2013) can then be used to calculate the OP values of the first time derivative of the continuous-time states,

$\dot{x}|_{op}$, constraint (algebraic) states, $z|_{op}$, and outputs, $y|_{op}$, for each module. Each of these variables can be perturbed (represented by Δ) about their respective OP values as given by Eq. 11 from Jonkman (2013) (e.g., for module inputs $u = u|_{op} + \Delta u$). Jonkman and Jonkman (2016) and Jonkman, Jonkman, and Platt (forthcoming) clarify how this operation is extended to rotations (orientations) in three dimensions, which do not reside in a linear space. The number of states, inputs and outputs (i.e., the size of the vectors x , x^d , z , u and y) depend on the features enabled in OpenFAST.

4.2.2 Module Linearization

As explained in Jonkman (2013), the FAST modularization framework supports a very general (need not be linear) state-space formulation, with any combination of continuous-time-state, discrete-time-state, constraint- (algebraic-) state, other- (e.g., logical) state, and output equations; however, for a module to support linearization, the formulation is limited to a hybrid semiexplicit differential-algebraic equation of index 1, which has the following limitations: (1) the continuous-time-state derivatives and discrete-time-state updates must be written as an explicit function of the states, inputs, and parameters; (2) the constraints must be of index 1; and (3) other states are used only for time-integration or when acting as parameters in the linearization process.

To support linearization, a module must also be able to export Jacobian matrices for the state and output equations with respect to the states and inputs. The OpenFAST module states, inputs, and outputs kept in the linearization process for the floating substructure flexibility and member-level load features linearized to date are summarized in Table 1. The OpenFAST module features linearized to date include only continuous-time and constraint states (no features with discrete-time states have yet been linearized).

The linearized form of a general module is given by Eq. 12 and 13 from Jonkman (2013); the forms for the land-based modules InflowWind, AeroDyn, ServoDyn, ElastoDyn, and BeamDyn are given in Jonkman and Jonkman (2016) and Jonkman, Jonkman, and Platt (forthcoming) and the forms for the prior linearization of offshore modules HydroDyn and MAP++ are given in Jonkman et al. (2018).

When adding floating substructure flexibility and member-level loads, the linearization of MAP++ is identical to what is given in Jonkman et al. (2018) and the linearization of HydroDyn is nearly identical to Jonkman et al. (2018), except that the state, input, and output vectors are of different size due to the existence of multiple potential-flow bodies (compare Table 1 in this report with Table 1 from Jonkman et al. (2018)). The resulting HydroDyn Jacobians contain the linearized contributions from: (1) state-space-based wave excitation for multiple potential-flow bodies; (2) hydrodynamic added mass; (3) state-space-based wave-radiation damping for multiple potential-flow bodies; (4) hydrostatic restoring (including from the strip-theory solution); and (5) linearized viscous drag. The linearization of SubDyn is new and given next.

The SubDyn module has continuous-time states, there are no restrictions to linearization, and the linearization form of the equations of motion and output equations is given by:

$$\Delta \dot{x}^{(SD)} = A^{(SD)} \Delta x^{(SD)} + B^{(SD)} \Delta u^{(SD)} \quad (54a)$$

$$\Delta y^{(SD)} = C^{(SD)} \Delta x^{(SD)} + D^{(SD)} \Delta u^{(SD)} \quad (54b)$$

Because SubDyn is inherently linear already, the linearization of SubDyn is straightforward. The continuous-state matrix, input matrix, continuous-state output matrix, and the input-transmission matrix are the Jacobians of the state and output equations relative to the states and inputs about the OP. The Jacobians of the state equations are implemented analytically and the Jacobians of the output equations are computed numerically via a central-difference perturbation technique, as shown in Eq. 55, which uses nomenclature from Damiani, Jonkman, and Hayman (2015)—where Ω_m is a diagonal matrix of eigenfrequencies of the retained C-B modes, ζ is a diagonal matrix of C-B mode damping ratios, \tilde{M}_{mB} is a partition of the substructure mass matrix after applying boundary constraints, and Φ_m^T is the transpose of the matrix containing the retained C-B eigenmodes—and where $X^{(SD)}$ is the continuous-state functions and $Y^{(SD)}$ is the output functions of SubDyn. The numerical processing of the output equations, which are already in a linear form, was selected for ease in processing the user-selected structural outputs (to minimize bookkeeping). For inputs that are rotations in three dimensions (i.e., $u = A$ and $\Delta u = \Delta \bar{\theta}$), it is implied that $u|_{op}^{(SD)} + \Delta u^{(SD)}$, $u|_{op}^{(SD)} - \Delta u^{(SD)}$ and $2\Delta u^{(SD)}$ are written as $f_{\Delta A} \left(f_{\Delta A}^{-1} \left(A|_{op}^{(SD)} \right) + \Delta \bar{\theta}^{(SD)} \right)$, $f_{\Delta A} \left(f_{\Delta A}^{-1} \left(A|_{op}^{(SD)} \right) - \Delta \bar{\theta}^{(SD)} \right)$ and $2\Delta \bar{\theta}^{(HD)}$, respectively. In Eq. 55a and 53 b, the column order is dictated by the order of SubDyn states and inputs and 0 and I are appropriately sized zero and identity matrices, respectively. For the numerically computed Jacobians, the default perturbation sizes are hard-coded within SubDyn (but can be customized by recompiling) and are ≈ 0.035 for states, ≈ 0.035 m for translational inputs, 2° for rotational inputs, ≈ 0.035 N for force inputs and ≈ 0.035 N-m for moment inputs. The Jacobians contain the contributions from mass, stiffness and damping of the substructure.

$$A^{(SD)} = \frac{\partial X}{\partial x} \Big|_{op}^{(SD)} = \begin{bmatrix} 0 & I \\ -\Omega_m^2 & -2\zeta\Omega_m \end{bmatrix} \quad (55a)$$

$$B^{(SD)} = \frac{\partial X}{\partial u} \Big|_{op}^{(SD)} = \begin{bmatrix} 0 & 0 & 0 \\ 0 & -\tilde{M}_{mB} & \Phi_m^T \end{bmatrix} \quad (55b)$$

$$C^{(SD)} = \frac{\partial Y}{\partial x} \Big|_{op}^{(SD)} = \frac{Y \left(x|_{op} + \Delta x, u|_{op}, t|_{op} \right) - Y \left(x|_{op} - \Delta x, u|_{op}, t|_{op} \right)}{2\Delta x} \Big|_{op}^{(SD)} \quad (55c)$$

$$D^{(SD)} = \frac{\partial Y}{\partial u} \Big|_{op}^{(SD)} = \frac{Y \left(x|_{op}, u|_{op} + \Delta u, t|_{op} \right) - Y \left(x|_{op}, u|_{op} - \Delta u, t|_{op} \right)}{2\Delta u} \Big|_{op}^{(SD)} \quad (55d)$$

4.2.3 Module-to-Module Coupling Linearization

The general approach to linearizing the mesh mapping within the module-to-module, input-output coupling relationships within OpenFAST, including rotations, is detailed in Jonkman and Jonkman (2016) and Jonkman, Jonkman, and Platt (forthcoming).

The linearized input-output transformation functions, U , are given by Eq. 8 from Jonkman and Jonkman (2016) or Eq. 15 from Jonkman (2013), repeated in Eq. 56 for convenience.

$$0 = \left. \frac{\partial U}{\partial \tilde{u}} \right|_{op} \Delta u + \left. \frac{\partial U}{\partial y} \right|_{op} \Delta y \quad \text{with} \quad \left. \frac{\partial U}{\partial \tilde{u}} \right|_{op} \neq 0 \quad (56)$$

As is evident from Table 1 and from Jonkman et al. (2018), the InflowWind, ServoDyn, ElastoDyn, AeroDyn, BeamDyn, HydroDyn, SubDyn, and MAP++ modules were developed so that for the most part—other than mapping between independent spatial discretizations—the

input of one module equals the output of another. It follows that with $U = \begin{Bmatrix} U^{(I/W)} \\ U^{(SrvD)} \\ U^{(ED)} \\ U^{(BD)} \\ U^{(AD)} \\ U^{(HD)} \\ U^{(SD)} \\ U^{(MAP)} \end{Bmatrix}$,

$$\Delta u = \begin{Bmatrix} \Delta u^{(I/W)} \\ \Delta u^{(SrvD)} \\ \Delta u^{(ED)} \\ \Delta u^{(BD)} \\ \Delta u^{(AD)} \\ \Delta u^{(HD)} \\ \Delta u^{(SD)} \\ \Delta u^{(MAP)} \end{Bmatrix} \quad \text{and} \quad \Delta y = \begin{Bmatrix} \Delta y^{(I/W)} \\ \Delta y^{(SrvD)} \\ \Delta y^{(ED)} \\ \Delta y^{(BD)} \\ \Delta y^{(AD)} \\ \Delta y^{(HD)} \\ \Delta y^{(SD)} \\ \Delta y^{(MAP)} \end{Bmatrix}, \quad \text{the Jacobian matrices evaluated at the OP from Eq. 56 for}$$

these seven modules are given by Eq. 57, where the sub-Jacobian matrices are composed of I s, 0 s, and the linearized matrices from the mapping transfers given in Jonkman and Jonkman (2016) and Jonkman, Jonkman, and Platt (forthcoming).

$$\left. \frac{\partial U}{\partial \bar{u}} \right|_{op} = \begin{bmatrix} I & 0 & 0 & 0 & \frac{\partial U^{(IW)}}{\partial \bar{u}^{(AD)}} & 0 & 0 & 0 \\ 0 & I & 0 & 0 & 0 & 0 & 0 & 0 \\ 0 & 0 & I & \frac{\partial U^{(ED)}}{\partial \bar{u}^{(BD)}} & \frac{\partial U^{(ED)}}{\partial \bar{u}^{(AD)}} & \frac{\partial U^{(ED)}}{\partial \bar{u}^{(HD)}} & \frac{\partial U^{(ED)}}{\partial \bar{u}^{(SD)}} & \frac{\partial U^{(ED)}}{\partial \bar{u}^{(MAP)}} \\ 0 & 0 & 0 & \frac{\partial U^{(BD)}}{\partial \bar{u}^{(BD)}} & \frac{\partial U^{(BD)}}{\partial \bar{u}^{(AD)}} & 0 & 0 & 0 \\ 0 & 0 & 0 & 0 & \frac{\partial U^{(AD)}}{\partial \bar{u}^{(AD)}} & 0 & 0 & 0 \\ 0 & 0 & 0 & 0 & 0 & \frac{\partial U^{(HD)}}{\partial \bar{u}^{(HD)}} & 0 & 0 \\ 0 & 0 & 0 & 0 & 0 & \frac{\partial U^{(SD)}}{\partial \bar{u}^{(HD)}} & \frac{\partial U^{(SD)}}{\partial \bar{u}^{(SD)}} & \frac{\partial U^{(SD)}}{\partial \bar{u}^{(MAP)}} \\ 0 & 0 & 0 & 0 & 0 & 0 & 0 & I \end{bmatrix}_{op} \quad (57a)$$

$$\left. \frac{\partial U}{\partial y} \right|_{op} = \begin{bmatrix} 0 & 0 & 0 & 0 & 0 & 0 & 0 & 0 & 0 \\ 0 & 0 & \frac{\partial U^{(SrvD)}}{\partial y^{(ED)}} & 0 & 0 & 0 & 0 & 0 & 0 \\ 0 & \frac{\partial U^{(ED)}}{\partial y^{(SrvD)}} & \frac{\partial U^{(ED)}}{\partial y^{(ED)}} & \frac{\partial U^{(ED)}}{\partial y^{(BD)}} & \frac{\partial U^{(ED)}}{\partial y^{(AD)}} & \frac{\partial U^{(ED)}}{\partial y^{(HD)}} & \frac{\partial U^{(ED)}}{\partial y^{(SD)}} & \frac{\partial U^{(ED)}}{\partial y^{(MAP)}} & 0 \\ 0 & 0 & \frac{\partial U^{(BD)}}{\partial y^{(ED)}} & \frac{\partial U^{(BD)}}{\partial y^{(BD)}} & \frac{\partial U^{(BD)}}{\partial y^{(AD)}} & 0 & 0 & 0 & 0 \\ \frac{\partial U^{(AD)}}{\partial y^{(IW)}} & 0 & \frac{\partial U^{(AD)}}{\partial y^{(ED)}} & \frac{\partial U^{(AD)}}{\partial y^{(BD)}} & 0 & 0 & 0 & 0 & 0 \\ 0 & 0 & \frac{\partial U^{(HD)}}{\partial y^{(ED)}} & 0 & 0 & 0 & \frac{\partial U^{(HD)}}{\partial y^{(SD)}} & 0 & 0 \\ 0 & 0 & \frac{\partial U^{(SD)}}{\partial y^{(ED)}} & 0 & 0 & \frac{\partial U^{(SD)}}{\partial y^{(HD)}} & \frac{\partial U^{(SD)}}{\partial y^{(SD)}} & \frac{\partial U^{(SD)}}{\partial y^{(MAP)}} & 0 \\ 0 & 0 & \frac{\partial U^{(MAP)}}{\partial y^{(ED)}} & 0 & 0 & 0 & \frac{\partial U^{(MAP)}}{\partial y^{(SD)}} & 0 & 0 \end{bmatrix}_{op} \quad (57b)$$

Because of their large size, the sub-Jacobian matrices are not shown here, but are described qualitatively instead:

- The first, second, fourth, and fifth equations of Eq. 56 for InflowWind inputs, $\theta = U^{(IW)}$, ServoDyn inputs, $\theta = U^{(SrvD)}$, BeamDyn inputs, $\theta = U^{(BD)}$, and AeroDyn inputs, $\theta = U^{(AD)}$, are described in Jonkman and Jonkman (2016), Jonkman, Jonkman, and Platt (forthcoming), and Jonkman et al. (2018).
- The third equation of Eq. 56 for ElastoDyn inputs, $\theta = U^{(ED)}$, is described in Jonkman and Jonkman (2016), Jonkman, Jonkman, and Platt (forthcoming), and Jonkman et al. (2018), except that when substructure flexibility is enabled, the equation now also includes terms expressing the contributions of SubDyn. That is, this equation expresses that the applied point force and moment perturbations distributed along the blades and tower as input to ElastoDyn are derived from the aerodynamic-applied line (per-unit length) force and moment perturbations distributed along the blades and tower as output from AeroDyn. This linearized load-mapping transfer also depends on the translational-displacement perturbations of analysis nodes along the blades and tower output from ElastoDyn. And when BeamDyn is enabled, point force and moment perturbations on the hub as input to

ElastoDyn are derived from the blade-root reaction point force and moment output from BeamDyn, which also depends on the translational-displacement perturbation of the hub reference point output from ElastoDyn. Additionally, the blade-pitch-angle-commands, nacelle-yaw-moment, and generator-torque perturbations as input to ElastoDyn are derived from the equivalent outputs from ServoDyn. The point force and moment perturbations on the transition piece as input to ElastoDyn are derived either from outputs of SubDyn or HydroDyn and MAP++, depending on whether the substructure is modeled flexibly or rigidly, respectively. When the substructure is modeled flexibly, the point force and moment perturbations on the transition piece as input to ElastoDyn are derived from the reaction point force and moment perturbations at the transition piece as output from SubDyn, which also depends on the translational-displacement perturbation of the transition piece output from ElastoDyn. When the substructure is modeled rigidly (within ElastoDyn), point force and moment perturbations on the transition piece as input to ElastoDyn are derived from the hydrodynamic-applied point force and moment perturbations distributed along the substructure as output from HydroDyn and the reaction point forces (tensions) lumped at each fairlead as output from MAP++, which also depends on the translational-displacement perturbation of the transition piece output from ElastoDyn.

- The sixth equation of Eq. 56 for HydroDyn inputs, $\theta = U^{(HD)}$, expresses that the translational displacement, orientation, translational and rotational velocity, and translational and rotational acceleration perturbations of analysis nodes distributed along the floating platform as input to HydroDyn are derived from motion outputs either from SubDyn or ElastoDyn, depending on whether the substructure is modeled flexibly or rigidly, respectively. For the former, the motion outputs at finite-element nodes distributed across the substructure from SubDyn are used; for the latter, the motion outputs at the transition piece from ElastoDyn are used.
- The seventh equation of Eq. 56 for SubDyn inputs, $\theta = U^{(SD)}$, expresses that translational displacement, orientation, translational and rotational velocity, and translational and rotational acceleration perturbations of the transition piece as input to SubDyn are derived from the motion outputs at the transition piece from ElastoDyn. Additionally, the applied point force and moment perturbations at finite-element nodes distributed along the substructure as input to SubDyn are derived from the hydrodynamic-applied point force and moment perturbations distributed along the substructure as output from HydroDyn and the reaction point forces (tensions) lumped at each fairlead as output from MAP++, which also depend on the translation-displacement perturbation of the finite-element nodes distributed across the substructure from SubDyn.
- The eighth equation of Eq. 56 for MAP++ inputs, $\theta = U^{(MAP)}$, expresses that the translational displacement perturbations of each fairlead as input to MAP++ are derived from the motion outputs either from SubDyn or ElastoDyn, depending on whether the substructure is modeled flexibly or rigidly, respectively. For the former, the motion outputs at finite-element nodes distributed across the substructure from SubDyn are used; for the latter, the motion outputs at the transition piece from ElastoDyn are used.

The Jacobian, $\left. \frac{\partial U}{\partial \tilde{u}} \right|_{op}$, has ones along its entire diagonal and it is easily shown that its determinant from Eq. 57 is nonzero.

4.2.4 Final Matrix Assembly

Once all individual modules and input-output relationships are linearized about the OP, the linearized model of the complete coupled system can be assembled. Linearization of the full-system model produces a linear state-space model representation of the complete nonlinear system about the OP, including the influence of system state and input perturbations on the system response and outputs. The general linearized form of the complete coupled system is

given by Eq. 18 and 19 from Jonkman (2013). With $\Delta x = \begin{Bmatrix} \Delta x^{(ED)} \\ \Delta x^{(BD)} \\ \Delta x^{(HD)} \\ \Delta x^{(SD)} \end{Bmatrix}$, the form for the OpenFAST

features linearized to date (without discrete-time states and with ElastoDyn, BeamDyn, and HydroDyn as the only modules with continuous-time states) is given by Eq. 58, where Δu^+ is the additional input perturbations (explained further in Jonkman (2013)).

$$\Delta \dot{x} = A\Delta x + B\Delta u^+ \quad (58a)$$

$$\Delta y = C\Delta x + D\Delta u^+ \quad (58b)$$

The full-system state-space matrices are given in Eq. 59, where $G|_{op}$ —explained more in Jonkman (2013) for the general case—for the OpenFAST linearization to date is given by Eq. 59. The matrix $G|_{op}$ has ones along its entire diagonal and it is easily shown that its determinant from Eq. 59 is nonzero, which means that the matrix inverse, $[G|_{op}]^{-1}$ from Eq. 59, exists and is bounded in the neighborhood around the OP.

$$A = \begin{bmatrix} A^{(ED)} & 0 & 0 & 0 \\ 0 & A^{(BD)} & 0 & 0 \\ 0 & 0 & A^{(HD)} & 0 \\ 0 & 0 & 0 & A^{(SD)} \end{bmatrix} - \begin{bmatrix} 0 & 0 & B^{(ED)} & 0 & 0 & 0 & 0 & 0 \\ 0 & 0 & 0 & B^{(BD)} & 0 & 0 & 0 & 0 \\ 0 & 0 & 0 & 0 & 0 & B^{(HD)} & 0 & 0 \\ 0 & 0 & 0 & 0 & 0 & 0 & 0 & B^{(SD)} \end{bmatrix} \left[G|_{op} \right]^{-1} \frac{\partial U}{\partial y} \Big|_{op} \begin{bmatrix} 0 & 0 & 0 & 0 \\ 0 & 0 & 0 & 0 \\ C^{(ED)} & 0 & 0 & 0 \\ 0 & C^{(BD)} & 0 & 0 \\ 0 & 0 & 0 & 0 \\ 0 & 0 & C^{(HD)} & 0 \\ 0 & 0 & 0 & C^{(SD)} \\ 0 & 0 & 0 & 0 \end{bmatrix} \quad (59a)$$

$$B = \begin{bmatrix} 0 & 0 & B^{(ED)} & 0 & 0 & 0 & 0 & 0 \\ 0 & 0 & 0 & B^{(BD)} & 0 & 0 & 0 & 0 \\ 0 & 0 & 0 & 0 & 0 & B^{(HD)} & 0 & 0 \\ 0 & 0 & 0 & 0 & 0 & 0 & 0 & B^{(SD)} \end{bmatrix} \left[G|_{op} \right]^{-1} \frac{\partial U}{\partial \ddot{u}} \Big|_{op} \quad (59b)$$

$$C = \begin{bmatrix} 0 & 0 & 0 & 0 \\ 0 & 0 & 0 & 0 \\ C^{(ED)} & 0 & 0 & 0 \\ 0 & C^{(BD)} & 0 & 0 \\ 0 & 0 & 0 & 0 \\ 0 & 0 & C^{(HD)} & 0 \\ 0 & 0 & 0 & C^{(SD)} \\ 0 & 0 & 0 & 0 \end{bmatrix} - \begin{bmatrix} D^{(MW)} & 0 & 0 & 0 & 0 & 0 & 0 & 0 \\ 0 & D^{(SvD)} & 0 & 0 & 0 & 0 & 0 & 0 \\ 0 & 0 & D^{(ED)} & 0 & 0 & 0 & 0 & 0 \\ 0 & 0 & 0 & D^{(BD)} & 0 & 0 & 0 & 0 \\ 0 & 0 & 0 & 0 & 0 & D^{(AD)} & 0 & 0 \\ 0 & 0 & 0 & 0 & 0 & 0 & D^{(HD)} & 0 \\ 0 & 0 & 0 & 0 & 0 & 0 & 0 & D^{(SD)} \\ 0 & 0 & 0 & 0 & 0 & 0 & 0 & D^{(MAP)} \end{bmatrix} \left[G|_{op} \right]^{-1} \frac{\partial U}{\partial y} \Big|_{op} \begin{bmatrix} 0 & 0 & 0 & 0 \\ 0 & 0 & 0 & 0 \\ C^{(ED)} & 0 & 0 & 0 \\ 0 & C^{(BD)} & 0 & 0 \\ 0 & 0 & 0 & 0 \\ 0 & 0 & C^{(HD)} & 0 \\ 0 & 0 & 0 & C^{(SD)} \\ 0 & 0 & 0 & 0 \end{bmatrix} \quad (59c)$$

$$D = \begin{bmatrix} D^{(IW)} & 0 & 0 & 0 & 0 & 0 & 0 & 0 \\ 0 & D^{(SrvD)} & 0 & 0 & 0 & 0 & 0 & 0 \\ 0 & 0 & D^{(ED)} & 0 & 0 & 0 & 0 & 0 \\ 0 & 0 & 0 & D^{(BD)} & 0 & 0 & 0 & 0 \\ 0 & 0 & 0 & 0 & D^{(AD)} & 0 & 0 & 0 \\ 0 & 0 & 0 & 0 & 0 & D^{(HD)} & 0 & 0 \\ 0 & 0 & 0 & 0 & 0 & 0 & D^{(SD)} & 0 \\ 0 & 0 & 0 & 0 & 0 & 0 & 0 & D^{(MAP)} \end{bmatrix} \left[G_{lop} \right]^{-1} \frac{\partial U}{\partial \bar{u}} \Big|_{lop} \quad (59d)$$

$$G_{lop} = \begin{bmatrix} I & 0 & 0 & 0 & \frac{\partial U^{(IW)}}{\partial \bar{u}^{(IW)}} & 0 & 0 & 0 \\ 0 & I & \frac{\partial U^{(SrvD)}}{\partial y^{(ED)}} D^{(ED)} & 0 & 0 & 0 & 0 & 0 \\ 0 & \frac{\partial U^{(ED)}}{\partial y^{(SrvD)}} D^{(SrvD)} & I + \frac{\partial U^{(ED)}}{\partial y^{(ED)}} D^{(ED)} & \frac{\partial U^{(ED)}}{\partial \bar{u}^{(BD)}} + \frac{\partial U^{(ED)}}{\partial y^{(BD)}} D^{(BD)} & \frac{\partial U^{(ED)}}{\partial \bar{u}^{(AD)}} + \frac{\partial U^{(ED)}}{\partial y^{(AD)}} D^{(AD)} & \frac{\partial U^{(ED)}}{\partial \bar{u}^{(HD)}} + \frac{\partial U^{(ED)}}{\partial y^{(HD)}} D^{(HD)} & \frac{\partial U^{(ED)}}{\partial \bar{u}^{(SD)}} + \frac{\partial U^{(ED)}}{\partial y^{(SD)}} D^{(SD)} & \frac{\partial U^{(ED)}}{\partial \bar{u}^{(MAP)}} + \frac{\partial U^{(ED)}}{\partial y^{(MAP)}} D^{(MAP)} \\ 0 & 0 & \frac{\partial U^{(BD)}}{\partial y^{(ED)}} D^{(ED)} & I + \frac{\partial U^{(BD)}}{\partial y^{(BD)}} D^{(BD)} & \frac{\partial U^{(BD)}}{\partial \bar{u}^{(AD)}} + \frac{\partial U^{(BD)}}{\partial y^{(AD)}} D^{(AD)} & 0 & 0 & 0 \\ 0 & \frac{\partial U^{(AD)}}{\partial y^{(IW)}} D^{(IW)} & 0 & \frac{\partial U^{(AD)}}{\partial y^{(ED)}} D^{(ED)} & I + \frac{\partial U^{(AD)}}{\partial y^{(AD)}} D^{(AD)} & 0 & 0 & 0 \\ 0 & 0 & \frac{\partial U^{(HD)}}{\partial y^{(ED)}} D^{(ED)} & 0 & 0 & I + \frac{\partial U^{(HD)}}{\partial y^{(HD)}} D^{(HD)} & \frac{\partial U^{(HD)}}{\partial y^{(SD)}} D^{(SD)} & 0 \\ 0 & 0 & \frac{\partial U^{(SD)}}{\partial y^{(ED)}} D^{(ED)} & 0 & 0 & \frac{\partial U^{(SD)}}{\partial \bar{u}^{(HD)}} + \frac{\partial U^{(SD)}}{\partial y^{(HD)}} D^{(HD)} & I + \frac{\partial U^{(SD)}}{\partial y^{(SD)}} D^{(SD)} & \frac{\partial U^{(SD)}}{\partial \bar{u}^{(MAP)}} + \frac{\partial U^{(SD)}}{\partial y^{(MAP)}} D^{(MAP)} \\ 0 & 0 & \frac{\partial U^{(MAP)}}{\partial y^{(ED)}} D^{(ED)} & 0 & 0 & 0 & \frac{\partial U^{(MAP)}}{\partial y^{(SD)}} D^{(SD)} & I \end{bmatrix} \quad (60)$$

with $|G_{lop}| \neq 0$

The input-transmission matrices impact all matrices of the linearized coupled system, highlighting the important role played by direct feedthrough of input to output in the coupled system response. For example, while the continuous-state matrix of ElastoDyn, $A^{(ED)}$, contains mass, stiffness, and damping only directly associated with the structural model of the wind turbine and tower, the full-system continuous state matrix, A , contains mass, stiffness, and damping associated with coupled aero-hydro-servo-elastics, including the wind turbine, tower, substructure and mooring system for floating offshore wind turbines.

When the linearized full-system matrices A , B , C , and D are exported to a file by OpenFAST, the additional input perturbations, Δu^+ , can be chosen by the user to be: (1) the inputs of all modules; (2) none of the module inputs (removing B and D from the file); or (3) a standard subset of these inputs, which include the standard wind turbine control inputs of nacelle-yaw moment, generator torque, and blade-pitch-angle commands (both independent and rotor-collective); the standard wind-inflow disturbances of horizontal wind speed, power-law shear exponent, and wind-propagation direction; and the standard incident-wave disturbance of wave elevation. Likewise, the output perturbations, Δy , can be chosen by the user to be: (1) the outputs of all modules; (2) none of the module outputs (removing C and D from the file); or (3) only the subset of output variables selected by the user through the OpenFAST module input files. Regardless of what the user selects to be exported to a file, all of the module inputs and outputs are used to form the linearized full-system matrices in Eq. 59, but only a subset of these matrices are exported based on the user selection.

5 Conclusions

This report presents the development of new capabilities in OpenFAST to model floating substructure flexibility and member-level loads to enable the design and optimization of the next-generation floating wind technologies that show promise to be streamlined, flexible, and cost-effective. Based on the structural dynamic and hydrodynamic modeling approaches and their coupling qualitatively presented in Jonkman et al. (2019), the mathematical details needed to understand and apply them correctly have been presented. It is envisioned that the new capability in OpenFAST will enable the design and optimization of advanced floating wind technologies. This implementation is part of a larger effort at NREL to develop an open-source, multifidelity systems-analysis capability for floating offshore wind turbine analysis and optimization that captures the relevant physics and costs that drive designs and trade-offs.

Verification of the source-code implementation is ongoing, and results will be presented in future work to highlight the functionality and demonstrate the verification.

References

Borg, M., A. M. Hansen, and H. Bredmose. 2016. “Floating Substructure Flexibility of Large-Volume 10-MW Offshore Wind Turbine Platforms in Dynamic Calculations.” *J. Physics: Conference Series, The Science of Making Torque from Wind (TORQUE 2016)*, 5–7 October 2016, Munich, Germany 082024 **753** <https://iopscience.iop.org/article/10.1088/1742-6596/753/8/082024/pdf>.

Cook, R. 1974. *Concepts and Applications of Finite Element Analysis*. Hoboken, New Jersey: John Wiley & Sons.

Damiani, R., J. Jonkman, and G. Hayman. 2015. *SubDyn User’s Guide and Theory Manual*. Golden, CO: National Renewable Energy Laboratory. NREL/TP-5000-63062. <https://www.nrel.gov/docs/fy15osti/63062.pdf>.

Jonkman, J. M. 2013. “The New Modularization Framework for the FAST Wind Turbine CAE Tool” *51st AIAA Aerospace Sciences Meeting including the New Horizons Forum and Aerospace Exposition*, 7–10 January 2013, Grapevine (Dallas/Ft. Worth Region), TX. AIAA-2013-0202 Reston, VA: American Institute of Aeronautics and Astronautics; NREL/CP-5000-57228 Golden, CO: National Renewable Energy Laboratory. <http://arc.aiaa.org/doi/pdf/10.2514/6.2013-202>.

Jonkman, J. M., R. R. Damiani, E. S. P. Branlard, M. Hall, G. J. Hayman, and A. N. Robertson. 2019. “Substructure Flexibility and Member-Level Load Capabilities for Floating Offshore Wind Turbines in OpenFAST.” *American Society of Mechanical Engineers (ASME) 2nd International Offshore Wind Technical Conference (IOWTC2019)*, 3–6 November 2019, St. Julian’s, Malta. IOWTC2019-7566 Houston, TX: The American Society of Mechanical Engineers (ASME International) Ocean, Offshore and Arctic Engineering (OOAE) Division. Golden, CO: National Renewable Energy Laboratory. NREL/CP-5000-74380. <https://asmedigitalcollection.asme.org/OMAE/proceedings/IOWTC2019/59353/St.%20Julian%E2%80%99s,%20Malta/1072009>.

Jonkman, J. M., and B. J. Jonkman. 2016. “FAST modularization framework for wind turbine simulation: full-system linearization.” *Journal of Physics: Conference Series, The Science of Making Torque from Wind (TORQUE 2016)*, 5–7 October 2016, Munich, Germany. 082010 **753**; Golden, CO: National Renewable Energy Laboratory. NREL/CP-5000-67015 <http://iopscience.iop.org/article/10.1088/1742-6596/753/8/082010/pdf>.

Jonkman, J. M., B. J. Jonkman, and A. Platt. Forthcoming. “Full-System Linearization for Wind Turbines with Aeroelastically Tailored Rotor Blades in OpenFAST.”

Jonkman, J., and M. Sprague. 2020. “OpenFAST.” Accessed April 26, 2019. <https://nwtc.nrel.gov/OpenFAST>.

Jonkman, J. M., A. D. Wright, G. J. Hayman, and A. N. Robertson. 2018. “Full-System Linearization for Floating Offshore Wind Turbines in OpenFAST.” *American Society of Mechanical Engineers (ASME) 1st International Offshore Wind Technical Conference (IOWTC2018)*, 4–7 November 2018, San Francisco, CA. IOWTC2018-1025 Houston, TX: The American Society of Mechanical Engineers (ASME International) Ocean, Offshore and Arctic Engineering (OOAE) Division. Golden, CO: National Renewable Energy Laboratory. NREL/CP-5000-71865.
<https://asmedigitalcollection.asme.org/OMAE/proceedings/IOWTC2018/51975/San%20Francisco,%20California,%20USA/275589>.

Johnson, N., J. Jonkman, A. Wright, and A. Robertson. 2019. “Verification of Floating Offshore Wind Linearization Functionality in OpenFAST.” *Journal of Physics: Conference Series: 16th Deep Sea Offshore Wind R&D Conference, EERA DeepWind'2019*, 16–18 January 2019, Trondheim, Norway. 012022 **1356**. Golden, CO: National Renewable Energy Laboratory. NREL/JA-5000-74210. DOI: 10.1088/1742-6596/1356/1/012022.
<https://iopscience.iop.org/article/10.1088/1742-6596/1356/1/012022/pdf>.

Lee, C. H., and J. N. Newman. 2006. *WAMIT User Manual, Versions 6.3, 6.3PC, 6.3S, 6.3S-PC* Chestnut Hill, MA: WAMIT, Inc.

Luan, C., Z. Gao, and T. Moan. 2017. “Development and verification of a time-domain approach for determining forces and moments in structural components of floaters with an application to floating wind turbines.” *Marine Structures* **51**: 87-109.
<https://www.sciencedirect.com/science/article/pii/S095183391630082X>.